KeAi
CHINESE ROOTS
GLOBAL IMPACT

Available online at www.sciencedirect.com

ScienceDirect

Advances in Climate Change Research 17 (2026) 1336−1350

www.keaipublishing.com/en/journals/accr/

Research

Changes in glacial lakes and associated risks in the China−Nepal Himalayas

Yu-Hong WU[a,b], Yong NIE[a,b,*], Wen WANG[a], Qi-Yuan LYU[a], Ming-Cheng HU[a,b], Muchu LESI[a,b], Hua-Yu ZHANG[a,b], Xu-Lei JIANG[a,b], Farooq AHMED[a,b]

[a] *Key Laboratory of Mountain Hazards and Engineering Resilience, Mountain Science Data Center, Institute of Mountain Hazards and Environment, Chinese Academy of Sciences, Chengdu 610213, China*

[b] *University of Chinese Academy of Sciences, Beijing 101408, China*

Received 23 November 2025; revised 24 May 2026; accepted 5 June 2026
Available online 12 June 2026

Abstract

The China−Nepal Himalayas (CNH) are threatened by glacial lake outburst floods (GLOFs), which endanger trade and local communities. Currently, glacial lake risk assessments in the CNH lack a reliable, quantitative, and cross-regional comparative approach. To fill this gap, this study presents a detailed and refined GLOF risk assessment using a data-driven machine learning framework. We first mapped lake boundaries in 1992, 2000, 2009, and 2022 using Landsat imagery and analyzed their distribution and temporal changes. We then identified potentially dangerous glacial lakes (PDGLs) among lakes that contact glaciers and are at least 0.1 km^2 in size. A machine learning model trained on High Mountain Asia estimated the likelihood that PDGLs would trigger GLOFs using key factors. We also evaluated impacts on exposed elements through stochastic inundation modeling. The final risk level was determined by combining hazard assessment with downstream impact analysis. Results show that 2377 glacial lakes were identified, mostly at elevations between 4100 m and 5900 m, with a 27% increase in area from 1992 to 2022. The trained model accurately identified all historical GLOFs in the CNH, confirming its high reliability. Downstream exposed elements, including buildings, bridges, roads, and hydropower facilities, remain at risk. Of the 76 lakes identified as potentially hazardous, four are categorized as having a very high risk and 14 as having a high risk. This study provides data to help stakeholders and policymakers pinpoint high-risk lakes and develop effective mitigation strategies.

Keywords: Glacial lake outburst floods; Climate change; Remote sensing; Downstream impact

1. Introduction

Glacial lakes are water bodies primarily formed through glacial processes (Nie et al., 2021), mainly from the meltwater of glaciers (Yao et al., 2012). These lakes are crucial freshwater sources in mountain regions (Cooley et al., 2021) and serve as sensitive indicators of climate change (King et al., 2019). Since the mid-20th century, earth's average surface temperature has increased by 0.16 °C per decade, with the High Mountain Asia (HMA) warming at nearly twice that rate (Yao et al., 2019). Rising temperatures accelerate glacier melting (Nie et al., 2025; Shugar et al., 2020), leading to the expansion of glacial lakes (Nie et al., 2023; Zhang et al., 2024). While this increases water storage, it raises the risk of glacial lake outburst floods (GLOFs) (Lesi et al., 2026; Taylor et al., 2023).

The China−Nepal Himalayas (CNH) is a globally vulnerable region for GLOF risks, particularly from moraine-

* Corresponding author. Key Laboratory of Mountain Hazards and Engineering Resilience, Mountain Science Data Center, Institute of Mountain Hazards and Environment, Chinese Academy of Sciences, Chengdu 610213, China.

E-mail address: nieyong@imde.ac.cn (NIE Y.).

Peer review under responsibility of National Climate Centre (China Meteorological Administration)

https://doi.org/10.1016/j.accre.2026.06.001

dammed lakes (Nie et al., 2013), with numerous documented events. Since 1960, 24 GLOFs have occurred, resulting in human casualties and economic damage (Lützow et al., 2023; Nie et al., 2018). The 1981 Cirenmaco GLOF destroyed infrastructures such as the China-Nepal Friendship Bridge, Sun Koshi hydropower plant, and highway (Khadka et al., 2018), killing over 200 people—one of the worst GLOFs in the Himalayas. The 2016 Gongbatongsha Co GLOF resulted in 70 million USD in damage to housing, transportation, and energy-exposed elements (Liu et al., 2020). These events highlight the urgent need for transboundary risk mitigation. Although GLOFs are infrequent (Nie et al., 2010), their sudden, rapid occurrence limits warning time, making mitigation difficult (Richardson and Reynolds, 2000). The region is developing infrastructure projects, including railways, hydropower, and trade routes, to enhance regional connectivity (Nie et al., 2023). Adopting science-based disaster risk assessment and prevention strategies is essential for sustainable development.

Although methodological advancements have shifted from qualitative to more quantitative techniques for glacial lake risk assessment (Zhou et al., 2024), current approaches (Zhang et al., 2023b; Zheng et al., 2021) still face challenges in reliability and generalizability. In hazard assessment, current research primarily employs semi-quantitative methods (De Brito and Evers, 2016), which classify risk levels based on quantitative indicators and qualitative weights. Yet, widely used classification approaches like natural breakpoints (Zheng et al., 2021) only rank relative risks within study areas, making direct comparisons across regions difficult (Allen et al., 2019). Meanwhile, quantitative evaluations provide objective estimates of hazard likelihood (Fischer et al., 2021) and directly yield an independent probability score for each lake's outburst. This score is independent of the classification of any specific sample set, enabling both standalone diagnosis of individual lakes and objective comparisons across regions. Frameworks exist for regions such as Gyirong, Poiqu (Gouli et al., 2025), and the Himalayas (Zhou et al., 2024), but most quantitative hazard research focuses on Himalayan GLOF events, neglecting the temporal gap between digital elevation model (DEM) generation and event occurrence, as well as sample reliability. Thus, it limits our understanding of glacial lake hazards. In downstream impact evaluation, studies utilize data on exposed elements from OpenStreetMap (OSM) (Wang et al., 2020a); however, coverage in the Third Pole region is limited. Reports suggest near-complete mapping in Nepal (Zhang et al., 2023b; Zheng et al., 2021), but high-resolution imagery monitoring reveals dramatic data gaps. Overall, these gaps in hazard and downstream impact assessments undermine the reliability and comparability of assessments across regions, hampering efforts to coordinate regional risk management. Therefore, developing a reliable risk assessment framework that ensures objective evaluation and comparability across domains is urgently needed.

This study aims to: 1) map the distribution of glacial lakes in the CNH and analyses their changes over time using Landsat images from 1992, 2000, 2009, and 2022; 2) apply a machine learning algorithm that automatically learns discriminant rules from carefully paired and temporally aligned historical samples, producing reliable, quantitative outburst probability estimates for PDGLs within the CNH; and 3) conduct a quantitative risk assessment that combines hazard data with socioeconomic exposure in flood-prone areas to enhance GLOF mitigation strategies. This study presents a reproducible, quantitative framework for assessing GLOF risk in the CNH. It identifies key lakes for mitigation and can be adapted to other regions with limited data, supporting climate adaptation and disaster risk reduction in the cryosphere.

2. Study area and data

2.1. Study area

The CNH, characterized by steep environmental gradients, diverse glacial lake types, an urgent need for coordinated risk management, and its importance within the Asian Water Tower, functions as an exemplary laboratory for developing a transferable risk assessment framework. We selected the CNH as the study area, which covers approximately 221876 km^2 and ranges in elevation from 60 to 8848 m above sea level, including approximately 6562 km^2 of glaciers (RGI 7.0 Consortium, 2023). The CNH (Fig. 1) is crucial to the China−Nepal Trade Corridor, which comprises key trade ports and vulnerable elements. However, it faces risks from transboundary natural disasters, particularly GLOFs. The CNH connects Tibet in China and Nepal, encompassing serveral trading ports, including Burang, Lizi, and Gyirong (Wu et al., 2022). The region exhibits complex terrain composed of mountain ranges and intermontane basins (Jiang et al., 2018), characterized by a distinct north-to-south topographical gradient (Hu et al., 2022). Most of the population resides in the southern regions (Gautam, 2017). The southern region has a subtropical monsoon climate, characterized by annual rainfall exceeding 1000 mm. In contrast, the northern area features a semi-arid climate with less than 400 mm of annual precipitation (Subba et al., 2024). Many glacial lakes in the area are classified as high risk (Allen et al., 2019; Zheng et al., 2021), posing serious risks to the local exposed elements. Research on glacial lake changes and associated GLOF risk is essential to advancing GLOF prevention and regional economic growth.

2.2. Data

A total of 246 Landsat images from the USGS Global Visualization Viewer (GloVis at https://glovis.usgs.gov/) were used for mapping and change analysis of glacial lakes (Fig. A1). The dataset included 55 scenes from Landsat-4/

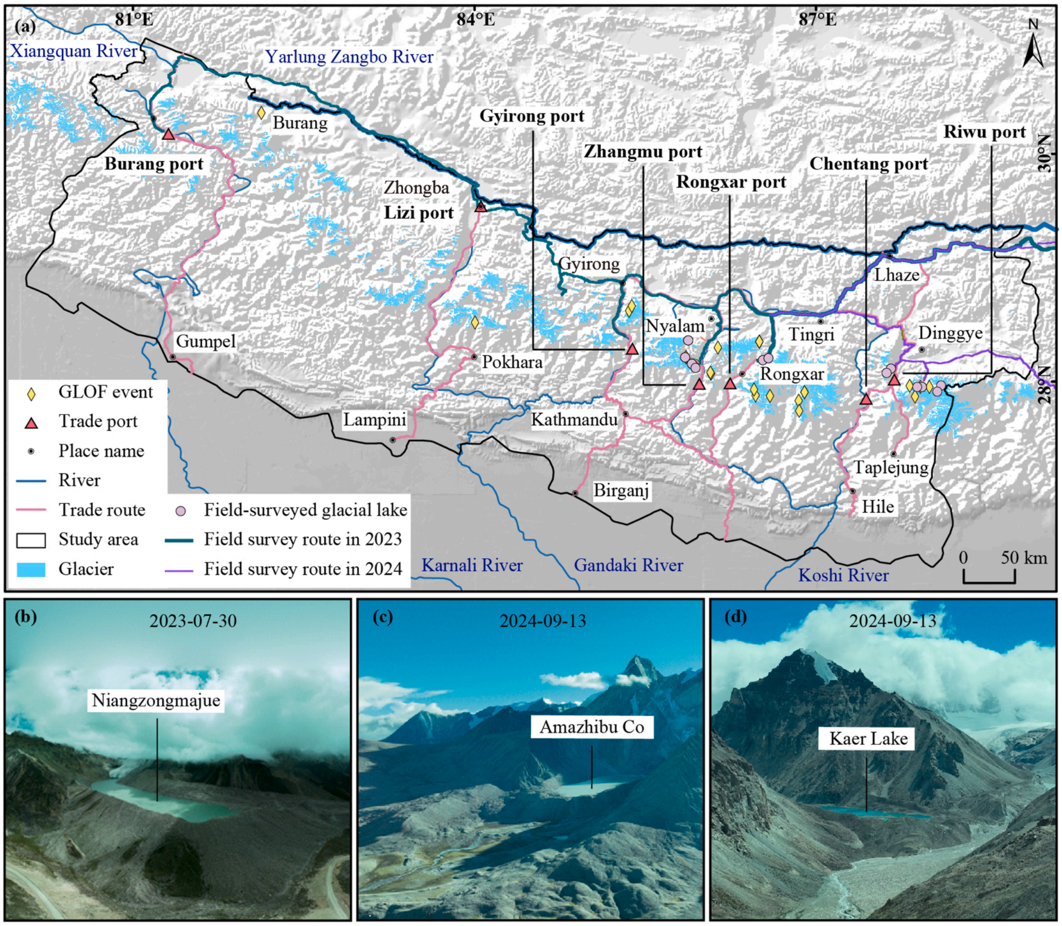

Fig. 1. Overview of the study area and field survey in the CNH. Location map showing glaciers, rivers, trade ports, routes, and field survey routes (a); photograph of Niangzongmajue (b), Amazhibu Co (c), and Kaer Lake (d).

5 TM for 1992, 66 scenes from Landsat-5 TM/Landsat-7 ETM+ for 2000, 56 scenes from Landsat-5 TM/Landsat-8 OLI for 2009, and 69 scenes from Landsat-8/9 OLI for 2022. Due to frequent cloud cover and snow interference, obtaining sufficient high-quality optical images for complete annual coverage was challenging (Nie et al., 2017). The year with the most available imagery was selected as the baseline, and images from adjacent years were incorporated to improve mapping accuracy and ensure complete coverage. All chosen images had less than 30% cloud cover (Nie et al., 2017). When cloud or seasonal snow obscured a target glacial lake in the initially selected image for a given period, it was replaced with a cloud-free alternative from an adjacent year. The four periods (circa 1992, 2000, 2009, and 2022) were selected based on data availability, as they yielded the largest number of Landsat images within their respective multi-year windows. Most images (62.60%) were acquired between September and November, with a focus on autumn changes in glacial lakes across the four periods (1992, 2000, 2009, and 2022). The Landsat images were Level-1 products. This product has been radiometrically calibrated and geometrically corrected by the USGS before distribution (Saunier et al., 2017). After downloading, we performed band stacking, which combines the individual spectral bands of each scene into a composite multispectral image.

The additional datasets included: 1) DEM data, 2) hydropower records, 3) a glacial lake inventory, 4) a GLOF inventory, 5) OSM geospatial data, 6) field survey data, and 7) meteorological data. The ALOS PALSAR DEM was sourced from the Alaska Satellite Facility Distributed Active Archive Center (https://asf.alaska.edu/, JAXA EORC, 2020) and processed to derive hazard assessment parameters and model potential flood extents for PDGLs. The DEM has a spatial resolution of 12.5 m and reported horizontal and vertical accuracies of approximately 4−8 m and 6−9 m, respectively (Adiri et al., 2022; Xu et al., 2024). Preprocessing involved mosaicking and voidfilling using nearest-neighbor resampling to maintain data completeness and geometric consistency (Trisakti and Julzarika, 2011). Two supplementary datasets, GloHydroRes (https://zenodo.org/records/14526360, Shah et al., 2025), and Global Dam Watch (https://www.globaldamwatch.org/directory Lehner et al., 2024), supported the identification and analysis of hydropower plants within potential flood zones. The glacial lake inventory (Song et al., 2025) identified glacial lakes across the HMA in 2022 that had no recorded GLOF events. Historical GLOF inventories

(Lützow et al., 2023; Nie et al., 2018) were used to select HMA lakes with documented GLOF events for machine learning. Data on geospatial-exposed elements from OSM (https://www.openstreetmap.org) were used to assess their exposure to the modeled GLOF regions. Field surveys were conducted in July 2023 and September 2024 to examine the dams, mother glaciers, geomorphological features, outlets, and downstream river channels of 12 representative glacial lakes, including Niangzongmajue, Amazhibu Co, and Kaer Lake (Fig. 1b–d). These lakes were selected to represent key risk gradients, with a focus on moraine-dammed lakes, the most prevalent and historically hazardous type in the study region. Field observations provided ground-truth data that validated remote-sensing-based dam-type classification and helped assess glacial-lake stability. Temperature and precipitation data (Yang et al., 2025) were used to analyze climate factors affecting glacial lake growth. These meteorological data, obtained from the Third Pole Environment Science Data Center (https://doi.org/10.11888/Atmos.tpdc.300398), were processed to calculate the annual average temperature and total annual precipitation from monthly data.

3. Methods

The workflow comprises five steps: analyzing the distribution and changes of glacial lakes, identifying PDGLs, estimating hazards, calculating downstream impacts, and assessing risk (Fig. 2).

3.1. Glacial lake inventory

3.1.1. Glacial lake mapping

The glacial lake was mapped using a semi-automated method that combined the normalized difference water index (NDWI) threshold (Nie et al., 2017; Wang et al., 2014). Post-processing of the glacial lake datasets included thorough quality control for each period. We verified the topology to ensure that water body boundaries were geometrically accurate. Next, we applied a size filter using a standard minimum mapping unit of 10,000 m^2 (~11 pixels) to exclude features smaller than this threshold from the final inventory. This approach ensured the consistency and reliability of the multi-temporal glacial lake records.

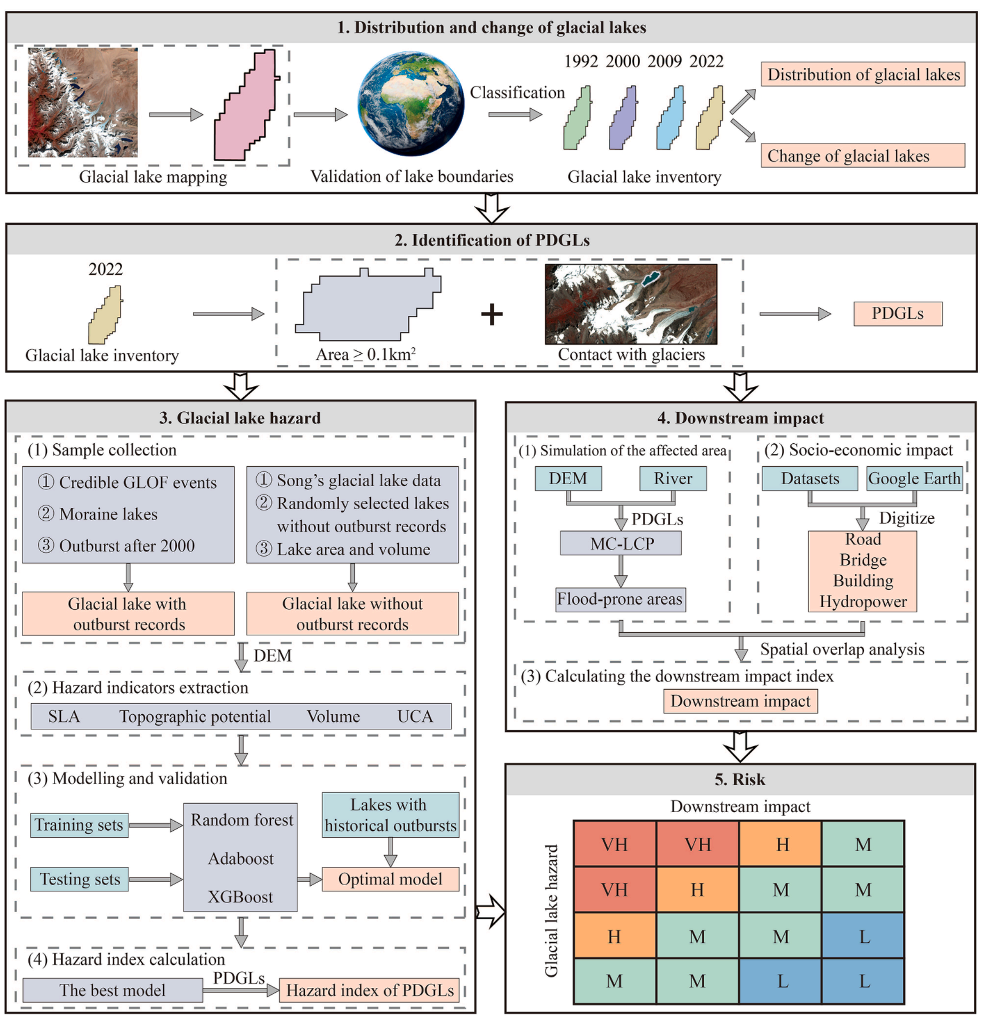

Fig. 2. Overview of the workflow on glacial lake change and risk assessment.

3.1.2. Validation of glacial lake boundaries

In 2022, 110 glacial lakes were randomly sampled for validation. Field surveys were difficult due to high altitudes; instead, high-resolution Google Earth imagery from 2022 and nearby years was used as a reference. Lakes were manually digitized from these images to verify Landsat-derived glacial lakes.

3.1.3. Glacial lake classification

All glacial lakes were manually classified through visual analysis of Landsat and Google Earth imagery or field surveys, based on their spatial relationships to upstream glaciers, as described in Lesi et al. (2022). The classification criteria are (Table 1): supraglacial lakes, which are water bodies on glacier surfaces; ice-contact lakes, directly touching the glacier; unconnected-glacier-fed lakes, supplied by glacial meltwater but not in direct contact; and non-glacier-fed lakes, with no visible hydrological connection to melting glaciers.

3.2. Identification of PDGLs

PDGLs are classified by lake size and type to assess risk. Lakes exceeding 10000 m^2 (Fan et al., 2019) can initiate destructive outburst floods that impact downstream regions. In the Himalayas, moraine-dammed lakes are most involved in such events (Gouli et al., 2025; Liu et al., 2020; Nie et al., 2018). Records (Lützow et al., 2023; Nie et al., 2018) indicate that most floods (15 of 19) originated from lakes that had been in contact with glaciers prior to failure. This study focused on glacier-contact moraine lakes as a crucial indicator for filtering PDGLs, emphasizing lakes that contact glaciers and exceed 10000 m^2 for detailed risk evaluation.

Table 1
Classification system for glacial lakes in the study area.

Lake type	Characteristic	Example in Landsat
Supraglacial	Lakes form on glacier surfaces, typically dammed by ice or weakly consolidated terminal moraines.	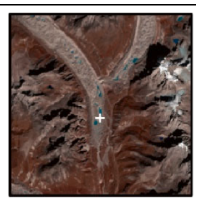
Ice-contact	Ice-contact lakes are directly dammed by glacial ice, terminal moraines, or bedrock, maintaining hydrological connectivity to glacier meltwater.	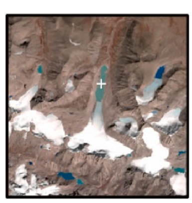
Unconnected-glacier-fed	Unconnected glacier-fed lakes receive indirect meltwater inputs from upstream glaciers but lack a direct connection to the glacier.	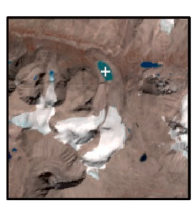
Non-glacier-fed lakes	Non-glacier-fed lakes formed by past glaciation are currently dammed by stabilized moraines or bedrock and are disconnected from contemporary meltwater inputs.	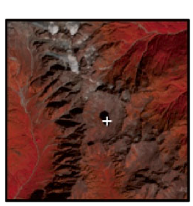

3.3. Glacial lake hazard

Calculating glacial lake hazard, which assesses the likelihood of a GLOF, includes sampling, parameter extraction, modeling, validation, and hazard index computation.

3.3.1. Sample collection

To build the model, we assembled a dataset of 37 moraine-dammed lakes with recorded outbursts and an equal number of lakes without GLOF records across the HMA. The GLOF collection involved three main steps: 1) selecting credible GLOF events from existing datasets (Lützow et al., 2023; Nie et al., 2018; Shrestha et al., 2023) to improve reliability; 2) focusing on moraine lakes as the primary GLOF sources; and 3) choosing lakes' outbursts after 2000 to match the production year of the DEM dataset. For lakes without outburst records, we: 1) obtained glacial lake boundaries from Song et al. (2025); 2) randomly selected lakes without recorded outbursts; and 3) refined these lakes using satellite images from 2022. To ensure data consistency and maintain an independent validation set, all CNH lakes with a history of outbursts were excluded from the training set. The lakes were evenly distributed across the HMA to improve representativeness (Fig. 3).

3.3.2. Hazard indicators extraction

Our hazard index incorporates four key parameters: steep lakefront area (SLA, reflecting moraine stability) (Fujita et al., 2008), topographic potential (indicating avalanche likelihood) (Allen et al., 2019), glacial lake volume (affecting flood severity) (Zhang et al., 2023a), and the upper catchment area (UCA, representing runoff contribution) (Wu et al., 2025). These were chosen for their objective derivation from DEMs and satellite imagery, independence from subjective interpretation, and statistical independence (Wangchuk et al., 2022). They reflect the main GLOF mechanisms, including ice avalanches, slope failures, moraine-dam instability, extreme rainfall, and hydrostatic forces (Emmer and Vilímek, 2014; Wangchuk and Bolch, 2020). Validated in prior susceptibility studies (Emmer and Vilímek, 2013; Khanal et al., 2015; Zhang et al., 2024), these indicators effectively predict glacial lake hazards.

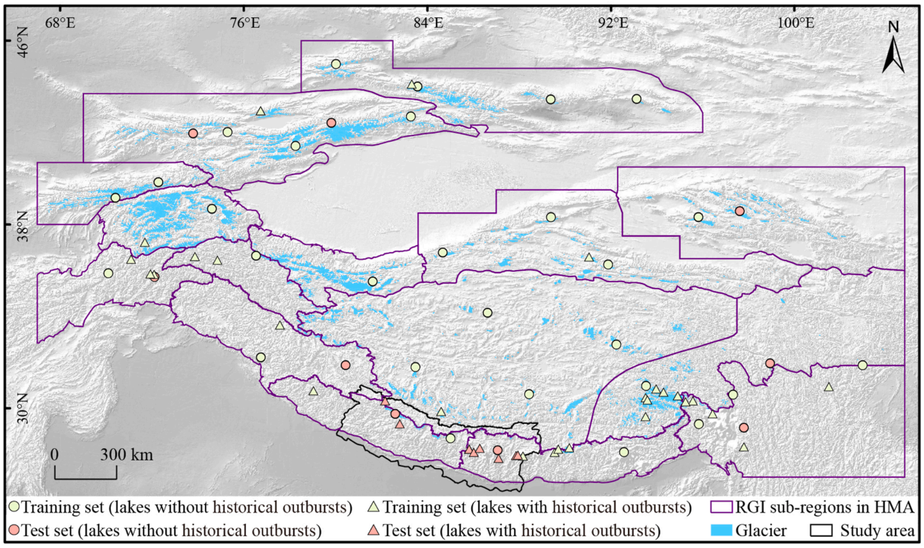

Fig. 3. Distribution of training and test samples of glacial lakes across the RGI sub-regions in the HMA.

3.3.3. Modeling and validation

(1) Modeling

Three machine learning algorithms—Random Forest (RF), Adaptive Boosting (AdaBoost), and Extreme Gradient Boosting (XGBoost)—were evaluated to identify the most effective model for detecting glacial lake hazards in CNH. We divided the dataset into training (75%) and test (25%) sets. The training set included twenty-eight glacial lakes with recorded GLOFs outside the CNH in the HMA, as well as twenty-eight lakes without GLOF records. The test set included nine lakes with recorded GLOFs in the CNH and nine lakes outside it. We employed binary classification to distinguish the classes and optimized hyperparameters across all machine learning algorithms to improve performance.

(2) Testing

Three objective metrics were used to assess the model's classification performance: the receiver operating characteristic−area under the curve (ROC-AUC) (Ben-David and Mandel, 1995), accuracy, and *F*-score (Roy et al., 2019). To evaluate the model's ability to generalize and stay stable with limited data while reducing overfitting, we used 10-fold stratified cross-validation on the training set (Kim, 2009). Paired *t*-tests compared models (Yildiz, 2013), performed only on training data to keep the test set independent for an unbiased final assessment. This method splits the data into 10 parts, trains on 9, validates on 1, and repeats this process to reduce bias. Significance was tested with paired *t*-tests; $p < 0.05$ indicated meaningful differences, indicating that the results were unlikely to be due to chance (White et al., 2022).

(3) Validation

For validation, we chose nine glacial lakes with known past outbursts in the study area. These lakes were used in the final model to predict future events and assess the model's reliability. The process compares predicted probabilities with observed data to assess accuracy, highlighting the model's ability to identify lakes with a history of outbursts.

3.3.4. Hazard index calculation

Our best model, selected for its accuracy, enabled us to estimate the GLOF susceptibility of PDGLs. We categorized the results into four hazard levels to facilitate interpretation. PDGLs with a probability of 0.75 or higher are considered ‘very high’, indicating a substantial threat of GLOF. Those with a probability between 0.5 and 0.75 are ‘high’, 0.25 to 0.5 are 'medium', and below 0.25 are ‘low’, implying a lower likelihood of GLOF. This classification helps policymakers prioritize their mitigation efforts by hazard level.

3.4. Downstream impact

Evaluating downstream impact involves examining how potential flooding affects exposed elements in the floodplain. This includes mapping flood-prone areas, analyzing exposed elements, identifying at-risk areas from GLOF runoff, and assessing threats to people, ecosystems, and assets to understand potential consequences.

3.4.1. Simulation of the affected area

We used the Monte Carlo Least Cost Path (MC-LCP) model (Watson et al., 2015), to simulate flood paths caused by PDGLs, accounting for DEM uncertainty across various Monte Carlo runs. MC-LCP calculated the flood probability for each grid cell across 500 iterations, accounting for DEM uncertainty at each iteration. We analyzed each PDGL using a 50 km cutoff to evaluate downstream impacts, as recommended by Dubey and Goyal (2020) and Taylor et al. (2023), and adjusted the cutoff if a large river or lake was within this distance.

3.4.2. Socio-economic impact

We assessed the effect of GLOFs on buildings, hydropower facilities, roads, and bridges. Initially, we used OSM data, but it had gaps, especially in rural and complex terrains. To improve this, we manually mapped the exposed elements affected by simulated GLOF paths to conduct a comprehensive assessment of their impact.

3.4.3. Calculating the downstream impact index

By overlaying corrected basic datasets with modeled inundation extents, we assessed the downstream effects of PDGLs. We normalized impact indicators—such as buildings, hydropower projects, roads, and bridges—on a 0-to-1 scale using Min-Max normalization, giving equal weights. For each PDGL, we calculated normalized values for all exposed elements within its impact zone and combined them into a composite exposure index to measure downstream impact. These were classified into four impact levels, corresponding to the hazard levels.

3.5. Risk

This study characterizes the risk of PDGLs as a matrix of hazards and downstream effects, as suggested by previous research (Chen et al., 2024; Zhang et al., 2023b; Zheng et al., 2021). All PDGLs are classified into four levels—very high, high, medium, and low—based on normalized values from the risk matrix. Our evaluation does not consider the vulnerability factor, which encompasses demographic traits, built-environment robustness, risk-mitigation measures, and socio-institutional capacity, as such data are unavailable in remote high-mountain regions.

4. Results

4.1. Distribution and change of glacial lakes

4.1.1. Mapping accuracy for glacial lakes

Our glacial lake boundaries, mapped using Landsat imagery, closely match higher-resolution reference data from Google Earth (Fig. A2). We are verifying the accuracy of our method and ensuring that our inventory is precise enough for trustworthy scientific use. The small differences between the two datasets lead to a mean area discrepancy of just 0.002 km^2 across all lakes. 92% of lakes fall within the 95% confidence interval, with a 6.59% overall area difference. This shows that our Landsat-based glacial lake inventory is sufficiently accurate for scientific uses such as monitoring changes and assessing risks.

4.1.2. Distribution of glacial lakes

Our inventory of 2377 glacial lakes in the CNH covers an area of 252.87 ± 26.04 km^2 as of 2022 (Fig. 4). Most lakes are along the Himalayan ridge, with smaller groups in the northeast. The Southern Himalayas have more lakes and a larger total area than the north. Glacier-fed lakes dominate (1334 lakes, 143.27 km^2), followed by ice-contact lakes (206 lakes, 72.47 km^2). Other lakes include 726 unconnected glacier-fed lakes (31.79 km^2) and supraglacial lakes. Ice-contact lakes are fewer but, on average, larger. In 2022, the lakes' average elevation was 5103 m (Fig. A3).

4.1.3. Change of glacial lakes

From 1992 to 2022, the number and area of glacial lakes in the CNH increased steadily. During this period, the number of lakes grew by 394, or 19.9%, and the total area expanded by 53.79 km^2, a 27.02% increase (Fig. A4a). The increase in area was mainly caused by large lakes ($\geq$1 km^2), while the fastest increase in lake numbers was observed in the smallest size category (0.01−0.05 km^2) (Fig. A4b). Growth occurred on both the southern and northern slopes, with the northern slope showing greater relative expansion (Fig. A4c). Among the different lake types, ice-contact lakes exhibited the largest increase in area, suggesting they are the most susceptible to climate change in the CNH (Fig. A5).

4.2. Hazard

4.2.1. Comparison of models

RF was chosen as the best model for hazard assessment due to its strong performance on the test set (Fig. 5). The training and test datasets have different distributions across hazard indicators, confirming the evaluation reflects the model's ability to generalize (Fig. A6). Cross-validation shows RF outperforms AdaBoost and XGBoost in ROC-AUC, accuracy, and *F*-score, with notable differences (Fig. A7). AdaBoost and XGBoost do not differ significantly in most metrics (Fig. A7). RF achieved the highest scores in ROC-AUC (0.91), accuracy (0.83), and *F*-score (0.83), indicating reliable predictions, and showed results consistent with AdaBoost and XGBoost.

4.2.2. Validation by historical GLOF events

Our validation focused on hazard index values for nine lakes with known historical outbursts, compared with 76 PDGLs (Fig. 6). For these lakes, the model estimated pre-outburst GLOF probabilities ranging from 0.56 to 0.95, with an average of 0.81. All nine were classified as high hazard—six as very high and three as high hazard. This correlation, in which lakes with past outbursts are assigned high predicted probabilities, highlights the model's

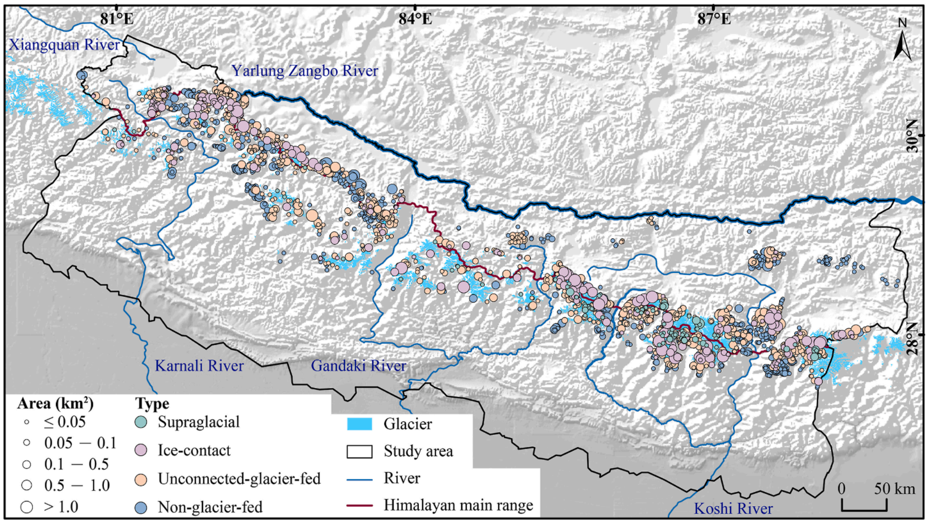

Fig. 4. Distribution of glacial lakes derived from Landsat images around 2022 in CNH.

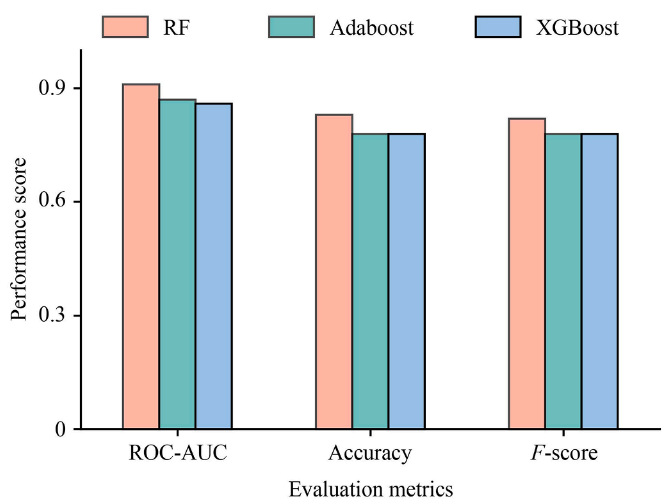

Fig. 5. Performance results of different models evaluated using test samples.

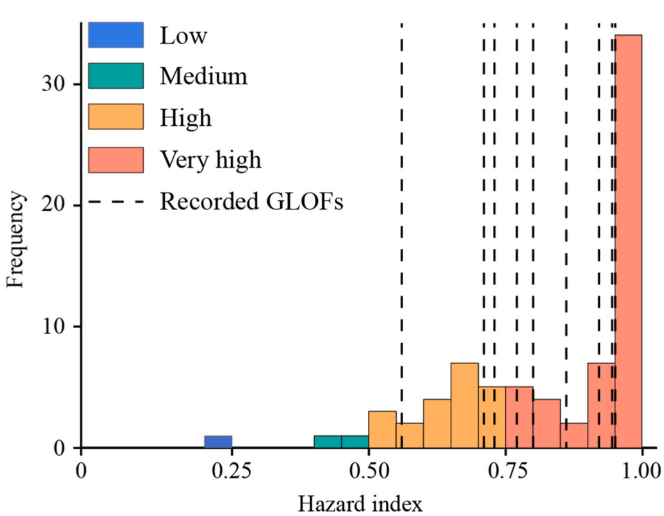

Fig. 6. Classification of hazard levels for PDGLs in CNH (Vertical dashed lines indicate the hazard index of 9 validated GLOFs).

effectiveness in assessing glacial lake hazards and supports its application to initial hazard screening.

4.2.3. Hazard assessment

Out of 76 PDGLs, 68.42% were considered as very high hazard, 27.63% were high, 2.63% were moderate, and 1.32% were low hazard (Fig. 7). Very high-hazard lakes tend to be larger, averaging 1.15 km^2, compared to 0.34 km^2 for high-hazard lakes, 0.12 km^2 for moderate-hazard lakes, and 0.11 km^2 for low-hazard lakes. Larger lakes, with more water and ice-contact boundaries, are more prone to calving and moraine destabilization. Since 96.05% of PDGLs are classified as high- or very-high hazard, they pose considerable risks to CNH.

4.3. Downstream impact

Two lakes showed very high impacts, three had high impacts, 19 had low impacts, and 52 had very low impacts (Fig. 8). The MC-LCP model produced detailed inundation maps for PDGLs. About 93.42% of PDGLs experienced low or very low impacts, mainly because no exposed elements were downstream. Most PDGL impact zones extend up to 50 km downstream, with notable variations in flood attenuation resulting from natural hydrological flow patterns. The Yarlung Tsangpo River receives flood discharges from PDGLs (e.g., Lake 31). In contrast, Paiku Co mitigates impacts from lakes such as Guoru Co and Guoqiang Co. These results help identify exposed elements along the flooding pathway, supporting risk assessment and mitigation planning.

Using high-resolution Google Earth imagery, we manually mapped exposed elements within potential inundation zones. This improves our ability to assess the downstream impacts of PDGLs in CNH. For example, Kimathanka Town (27.8650°N, 87.4214°E), where the original and revised datasets clearly differ (Fig. 9),

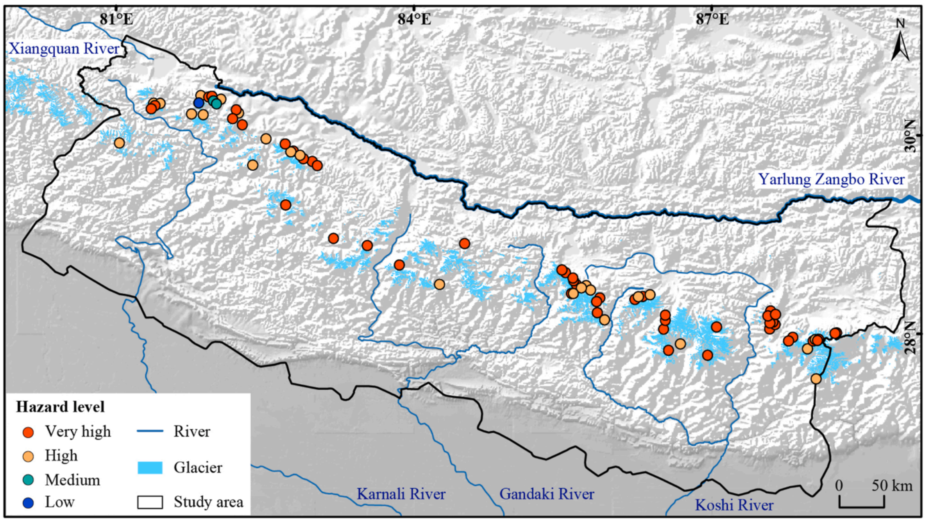

Fig. 7. Distribution of PDGLs with different hazard levels across CNH.

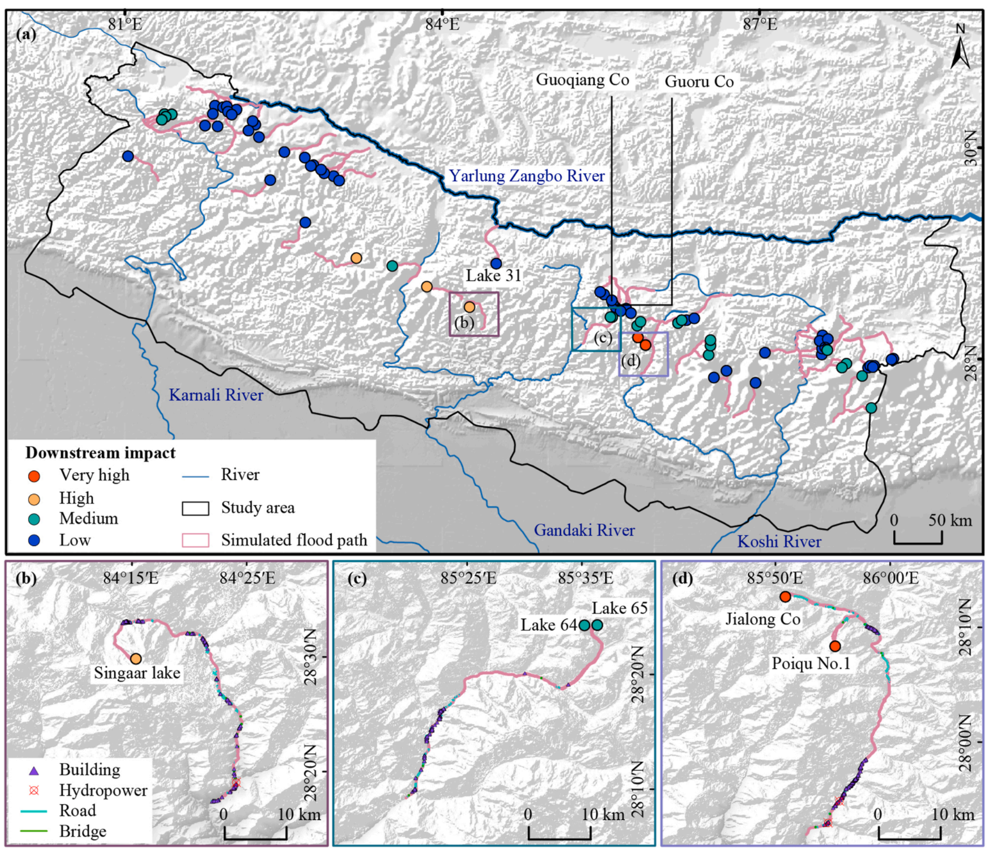

Fig. 8. Distribution of PDGLs with varying impacts across the CNH (a), the inundation probability estimated by MC-LCP for Singaar Lake (b), lakes 64 and 65 (c), and Jialong Co and Poiqu No.1 (d).

highlights the importance of these updates. This study identified highly exposed elements in CNH, including 0.39 km^2 of buildings, 260.38 km of roads, and 9.35 km of bridges (Table 2). This dataset provides a more accurate analysis of elements at risk, addressing the limitations of existing data that underestimate the number of exposed elements in remote Himalayan valleys.

4.4. Risk assessment

Our analysis showed that within the CNH, four lakes were classified as very high risk, fourteen as high risk, fifty-five as medium risk, and three as low risk (Fig. 10). Four lakes, including Peace Lake, Tilicho Lake, Jialong Co, and Poiqu No.1, were at very high risk, located at elevations

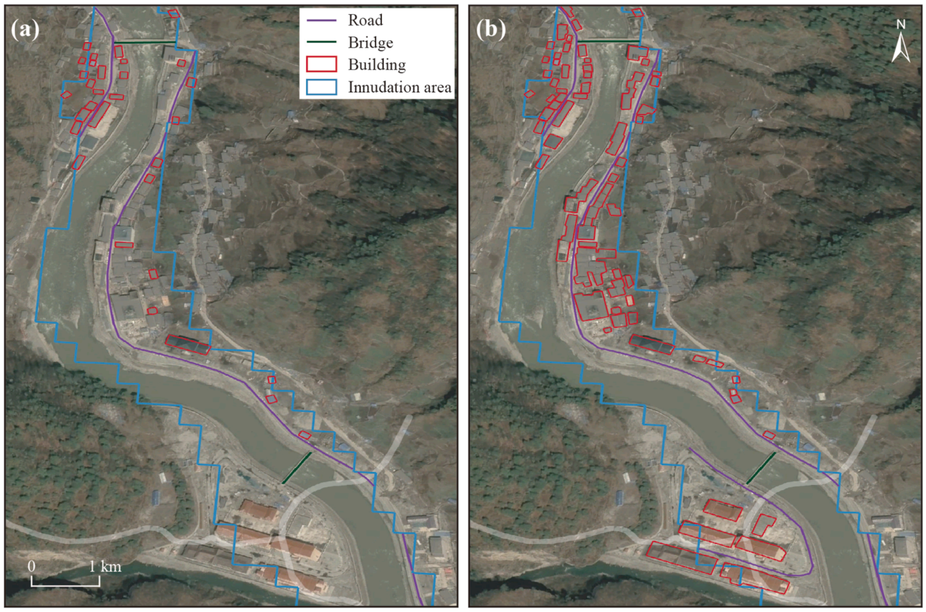

Fig. 9. Kimathanka town (27.8650°N, 87.4214°E) was selected to demonstrate uncorrected (a) and corrected (b) exposed elements located downstream from PDGLs.

Table 2
Comparison of corrected and uncorrected exposed elements.

Type	Building (km^2)	Road (km)	Bridge (km)	Hydropower (count)
Uncorrected	0.27	225.67	8.81	4
Corrected	0.39	260.38	9.35	9
Difference	0.12	34.71	0.54	5

between 4426 and 5532 m, and covered 4.59 km^2. Many high-risk lakes have expanded over the past decades, increasing instability and the risk of outbursts. Low- and medium-risk PDGLs typically have limited exposed elements downstream, which lowers their risk.

5. Discussion

5.1. Glacial lake mapping, changes, and their climatic drivers

We selected 110 validation lakes from the 2022 glacial lake inventory, representing a range of sizes, elevations, and main types, excluding rapidly changing supraglacial lakes to ensure stability (Fig. A8). These lakes are evenly spread across the study area to prevent geographical bias. We manually examined the historical imagery timeline for each validated lake and selected images up to 2022 (Wang et al., 2020b). This approach is common in glacial lake validation (Deng et al., 2025; Zhang et al., 2026).

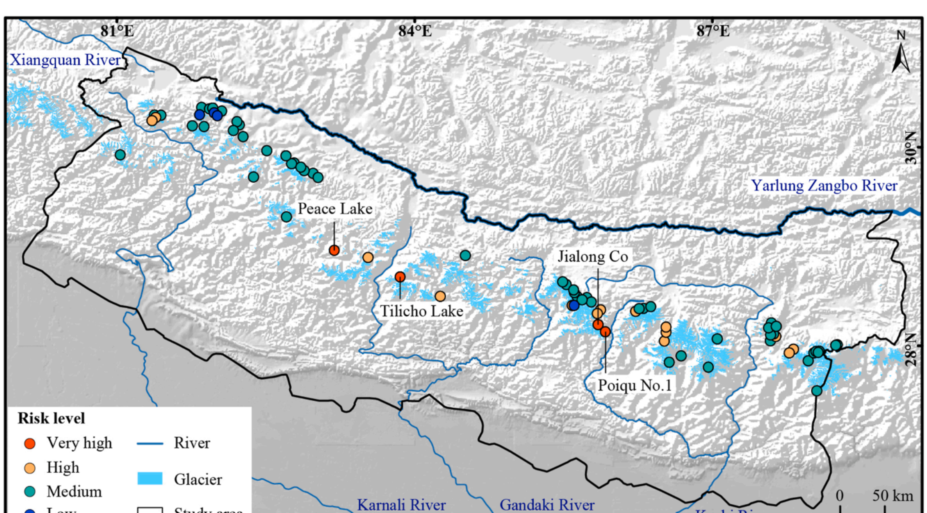

Fig. 10. Distribution of glacial lakes with varying risk levels across the CNH.

We selected 1992, 2000, 2009, and 2022 as key benchmarks for analyzing glacial lake changes based on the number of Landsat images available for each year. When cloud or snow cover hindered extraction, we used nearby images within a ±1- to ±2-year window (Nie et al., 2017). This approach is justified because most non-supraglacial lakes have stable boundaries over short timescales (Deng et al., 2025), and using only images from the same year would result in fragmented and unreliable data (Zhang et al., 2026).

Rising temperatures have led to glacier retreat and increased meltwater inflow into lakes (Zhang et al., 2019), causing glacial lakes to expand from 1992 to 2022 (Fig. A9). The average temperature rose by 0.23 °C per decade, annual precipitation increased by 47.84 mm, and the area of glacial lakes expanded by 53.80 km^2. Elevated temperatures have accelerated glacier melting and retreat (Dehecq et al., 2019), and increased meltwater and rainfall have directly supplied water to the lakes (Marzeion et al., 2014).

5.2. Glacial lake hazard

5.2.1. Influence of DEM uncertainty on hazard indicators

DEM-derived parameters (SLA, UCA, and topographic potential) are affected by uncertainties inherent in the DEM. We corrected the systematic bias in UCA using visual interpretation (Wu et al., 2025). DEM vertical errors directly affect SLA estimates, particularly for low-height dams (Fujita et al., 2013), and may misclassify steep slopes, thereby affecting topographic potential (Allen et al., 2019). Future work should use higher-precision topographic data or field surveys to minimize these uncertainties.

5.2.2. The empirical formulae of lake volume

Estimating glacial lake volumes using empirical formulas carries some uncertainty. Nevertheless, the formula we employed was specifically developed for Himalayan glacial lakes (Zhang et al., 2023a), which helps minimize systematic errors and outperforms other methods. Consequently, the volume estimates are sufficiently reliable for regional hazard assessments (Qi et al., 2025). While limited field data hinder direct validation, this empirical approach provides a practical solution (Qi et al., 2022). In the future, as more water-depth data becomes available, the formula can be refined to improve accuracy.

5.2.3. The sample size and validation sets

Our sample includes 37 outbursts and 37 non-outburst lakes, carefully selected for quality despite limited numbers. Rigorous cross-validation and multi-level screening (e.g., ensuring events post-date DEM, cross-checking primary sources) produced 37 high-confidence events. Recent research across different sample sizes, such as Gouli et al. (2025) with 51 events, Liu et al. (2025) with 66, and Zhou et al. (2024) with 54, confirms the reliability of these sample sizes. The repeated 10-fold cross-validation (Kim, 2009) enhances model stability and reduces overfitting. Future work should apply this rigorous validation approach to larger global datasets to improve model robustness.

To evaluate spatial extrapolation, we used a geographically isolated approach, in which nine GLOF events in the CNH were omitted from the training set to form an independent validation set. Even if local feature distributions overlap during application, this method remains valid as long as validation samples are geographically distinct from the training region (Wenger and Olden, 2012).This method is widely used in hazard modeling (Goetz et al., 2021; Gouli et al., 2025; Kumar et al., 2025) and is used to test model performance in new geographic regions (Roberts et al., 2017).

5.2.4. The selected hazard indicators

Our hazard assessment uses four key indicators (SLA, topographic potential, lake volume, UCA) that are widely adopted (Allen et al., 2019; Chen et al., 2024; Zheng et al., 2021) and closely linked to failure mechanisms (Emmer and Vilímek, 2013). These parameters are selected based on data availability and regional consistency, eliminating the need for locally variable dynamic data (Allen et al., 2019). Validation against historical events confirms their accuracy.

5.2.5. Comparison with other studies

Our glacial lake hazard assessment closely aligns with prior research. Lakes designated as very high hazard (Gouli et al., 2025; Zhang et al., 2024)—such as Galong Co (28.3223°N, 85.8381°E) and Niangzongmajue (28.1853°N, 86.5321°E)—were also classified as very high hazard in our study. Our results concur with earlier evaluations (Zhang et al., 2023b; Zheng et al., 2021). Among the 73 lakes identified as high or very high hazard, Zhang et al., 2023b recognized 67, while Zheng et al. (2021) identified 58 as very high or high hazard (Table A1). This agreement across multiple independent studies confirms the robustness of our hazard assessment framework and strengthens confidence in our findings.

5.3. Downstream impact

The downstream impact assessment is affected by DEM uncertainty, the simulation model, and the weighting of exposed elements.

5.3.1. The effect of DEM uncertainty

DEM uncertainties affect downstream impact assessments by altering flood simulations, potentially leading to overestimation or underestimation of the elements affected. Our MC-LCP model incorporates uncertainty assessment and is minimally affected by DEM quality (Watson et al., 2015), enhancing result reliability. The ALOS PALSAR DEM was processed via the nearest-neighbor resampling method, which has a negligible impact on the downstream flood simulation (Shen and Tan, 2020). Future studies could improve accuracy using high-resolution commercial satellite DEMs.

5.3.2. Affected-area simulation

The MC-LCP model is well-suited to large-area applications due to its computational efficiency. Physical models are better suited to localized engineering assessments but require key parameters (e.g., channel roughness, high-resolution topography) that are difficult to obtain regionally (Yang et al., 2023). Future work should include field surveys and high-resolution hydrodynamic modeling at critical sites.

We used a 50 km channel-length threshold for flood-propagation analysis, based on typical GLOF impact distances (Rafiq et al., 2019; Watson et al., 2015). This fixed 50 km threshold provides a practical way to prioritize downstream impacts (Dubey and Goyal, 2020; Rounce et al., 2017; Taylor et al., 2023), although it may underestimate very large events (Sattar et al., 2025). Future improvements could use empirical formulas that relate lake area to impact distance.

5.3.3. Weighting of exposed elements

Buildings, roads, bridges, and hydropower projects were treated equally when assessing downstream exposure to potential glacial lake outburst floods. Assigning different weights would introduce subjectivity and uncertainty (Zheng et al., 2021), as these assets serve different social and economic roles. Equal weights provide an objective, consistent approach and reduce subjective disagreements about weights. Future research could incorporate stakeholder input to adjust weights for specific decision-making contexts.

5.4. Advantages and limitations

We have developed a more reliable framework for quantitatively assessing the risk of glacial lakes. By expanding and carefully curating historical data, we constructed a dataset that more accurately reflects actual conditions, enhancing assessment precision. The framework integrates high-resolution imagery to incorporate detailed exposure data, providing accurate spatial information for evaluation. Compared with earlier quantitative methods (Gouli et al., 2025), our results offer greater dependability. Unlike earlier wide-area risk assessments (Zheng et al., 2021), our data-driven approach facilitates cross-regional comparisons, supporting collaborative risk management.

Our framework provides a practical, cost-effective approach to assessing GLOF risk in data-scarce regions, such as the CNH. It enables rapid identification of high-risk lakes for targeted field investigations and produces hazard-impact maps to support decision-making (Gouli et al., 2025). Future research should prioritize on-site investigations of these lakes, considering triggers, vulnerability, and resilience, and employ probabilistic and physically based modeling for critical lakes. This study's transboundary coverage of the CNH reveals cross-border heterogeneity in lake evolution, data availability, and downstream exposure. This cross-border aspect is notable. To improve future cross-regional assessments, we recommend harmonized lake inventories, shared high-resolution DEMs, and joint field surveys across the China−Nepal border. Limitations include DEM inaccuracies, limited historical GLOF records, potential underestimation of extreme inundation, and the absence of societal resilience factors. Future work should use higher-resolution data, expand the outburst database, integrate hydrodynamic modeling with field verification, and incorporate socioeconomic indicators.

6. Conclusions

This study integrates remote sensing, machine learning, and modeling to quantitatively assess glacial lake changes and GLOF risk in the CNH. We mapped the spatial distribution and changes of glacial lakes, optimized the glacial lake risk assessment framework, and applied stochastic flood modeling to estimate downstream impacts.

Our analysis shows dramatic changes in the glacial lake inventory over 30 years. The number of lakes rose from 1983 to 2377, and the total area increased from 199.07 km^2 to 252.87 km^2. Ice-contact lakes saw the largest growth (25.52 km^2), while unconnected glacier-fed lakes added 234 new lakes. These trends reflect different responses to climate warming; ice-contact lakes are especially vulnerable to glacier retreat. These findings help understand cryospheric hydrology by linking lake types to glacial processes and provide a baseline for hazard assessment and climate adaptation.

This study advances GLOF risk assessment by analyzing 76 PDGLs in the CNH. The results demonstrate that the RF model surpasses AdaBoost and XGBoost in GLOF susceptibility mapping. Notably, the analysis highlights four lakes at very high risk and 14 at high risk, marking the quantitative prioritization of sites needing urgent mitigation in the CNH. These insights improve risk mitigation by more accurately identifying vulnerable areas. The standardized risk assessment framework provides reproducible and comparable results, creating a solid baseline for future research and regional comparisons. Overall, these findings offer valuable scientific support for climate adaptation and disaster mitigation efforts in this mountainous region, where data are limited. Additionally, this glacial lake risk assessment framework is designed to be adaptable to other regions with limited data, enabling reproducible GLOF susceptibility mapping and site prioritization beyond the CNH.

Declaration of competing interest

The authors declare no conflict of interest.

CRediT authorship contribution statement

Yu-Hong Wu: Writing – original draft, Methodology, Formal analysis, Conceptualization. **Yong Nie:** Writing – review & editing, Supervision, Project administration, Funding acquisition, Conceptualization. **Wen Wang:** Writing – review & editing, Methodology, Data curation. **Qi-Yuan Lyu:** Data curation. **Ming-Cheng Hu:** Resources, Methodology. **Muchu Lesi:** Writing – review & editing, Visualization, Validation. **Hua-Yu Zhang:** Writing – review & editing. **Xu-Lei Jiang:** Resources, Data curation. **Farooq Ahmed:** Writing – review & editing.

Declaration of generative AI use

During the preparation of this work, the authors did not use any AI tools.

Acknowledgments

This work was funded by the National Key Research and Development Program of China (2025YFE0211403), the Science and Technology Department of Tibet (XZ202601ZY0049), and the Key Laboratory of Mountain Hazards and Engineering Resilience, Chinese Academy of Sciences (KLMHER-T04). We would like to thank GloVis, ASF, and the OpenStreetMap Foundation for providing archival Landsat images, the ALOS-PALSAR DEM, and OSM geospatial data, respectively.

Appendix A. Supplementary data

Supplementary data to this article can be found online at https://doi.org/10.1016/j.accre.2026.06.001.

References

Adiri, Z., Lhissou, R., Maacha, L., et al., 2022. Comparison of ASTER GDEM3, SRTM3, NASADEM, TanDEM-X90, AW3D30, and ALOS PALSAR data with TanDEM-X12: a case study of Tagragra of Akka inlier, Moroccan Anti-Atlas. Arabian J. Geosci. 15 (21), 1654.

Allen, S.K., Zhang, G., Wang, W., et al., 2019. Potentially dangerous glacial lakes across the Tibetan Plateau revealed using a large-scale automated assessment approach. Sci. Bull. 64 (7), 435–445.

Ben-David, A., Mandel, J., 1995. Classification accuracy: machine learning vs. explicit knowledge acquisition. Mach. Learn. 18 (1), 109–114.

Chen, M., Chen, Y., Fang, G., et al., 2024. Risk assessment of glacial lake outburst flood in the Central Asian Tienshan Mountains. npj Clim. Atmos. Sci. 7 (1), 209.

Cooley, S.W., Ryan, J.C., Smith, L.C., 2021. Human alteration of global surface water storage variability. Nature 591 (7848), 78–81.

De Brito, M.M., Evers, M., 2016. Multi-criteria decision-making for flood risk management: a survey of the current state of the art. Nat. Hazards Earth Syst. Sci. 16 (4), 1019–1033.

Dehecq, A., Gourmelen, N., Gardner, A.S., et al., 2019. Twenty-first century glacier slowdown driven by mass loss in High Mountain Asia. Nat. Geosci. 12 (1), 22–27.

Deng, Q., Nie, Y., Carrivick, J.L., et al., 2025. A 10-m glacial lake dataset along the Sichuan-Tibet Railway using Sentinel-2 images. Geo Spatial Inf. Sci.

Dubey, S., Goyal, M.K., 2020. Glacial lake outburst flood hazard, downstream impact, and risk over the Indian Himalayas. Water Resour. Res. 56 (4) e2019WR026533.

Emmer, A., Vilímek, V., 2013. Review article: lake and breach hazard assessment for moraine-dammed lakes: an example from the Cordillera Blanca (Peru). Nat. Hazards Earth Syst. Sci. 13 (6), 1551–1565.

Emmer, A., Vilímek, V., 2014. New method for assessing the susceptibility of glacial lakes to outburst floods in the Cordillera Blanca, Peru. Hydrol. Earth Syst. Sci. 18 (9), 3461–3479.

Fan, J., An, C., Zhang, X., et al., 2019. Hazard assessment of glacial lake outburst floods in Southeast Tibet based on RS and GIS technologies. Int. J. Rem. Sens. 40 (13), 4955–4979.

Fischer, M., Korup, O., Veh, G., et al., 2021. Controls of outbursts of moraine-dammed lakes in the greater Himalayan region. Cryosphere 15 (8), 4145–4163.

Fujita, K., Sakai, A., Takenaka, S., et al., 2013. Potential flood volume of Himalayan glacial lakes. Nat. Hazards Earth Syst. Sci. 13 (7), 1827–1839.

Fujita, K., Suzuki, R., Nuimura, T., et al., 2008. Performance of ASTER and SRTM DEMs, and their potential for assessing glacial lakes in the Lunana region, Bhutan Himalaya. J. Glaciol. 54 (185), 220–228.

Gautam, D., 2017. Assessment of social vulnerability to natural hazards in Nepal. Nat. Hazards Earth Syst. Sci. 17 (12), 2313–2320.

Goetz, J., Kohrs, R., Parra Hormazábal, E., et al., 2021. Optimizing and validating the gravitational process path model for regional debris-flow runout modelling. Nat. Hazards Earth Syst. Sci. 21 (8), 2543–2562.

Gouli, M.R., Hu, K., Khadka, N., et al., 2025. Quantitative assessment of the GLOF risk along China-Nepal transboundary basins by integrating remote sensing, machine learning, and hydrodynamic model. Int. J. Disaster Risk Reduction 118, 105231.

Hu, J., Yao, X., Duan, H., et al., 2022. Temporal and spatial changes and GLOF susceptibility assessment of glacial lakes in Nepal from 2000 to 2020. Remote Sens. 14 (19), 5034.

JAXA EORC, 2020. ALOS Global Digital Surface Model (DSM). ALOS World 3D-30m (AW3D30). Version 3.1 (Product Description). Earth Observation Res. Center, Japan Aerospace Explor. Agency (JAXA EORC).

Jiang, S., Nie, Y., Liu, Q., et al., 2018. Glacier change, supraglacial debris expansion and glacial lake evolution in the Gyirong River Basin, Central Himalayas, between 1988 and 2015. Remote Sens. 10 (7), 986.

Khadka, N., Zhang, G., Thakuri, S., 2018. Glacial lakes in the Nepal Himalaya: inventory and decadal dynamics (1977-2017). Remote Sens. 10 (12), 1913.

Khanal, N.R., Hu, J., Mool, P., 2015. Glacial lake outburst flood risk in the Poiqu/Bhote Koshi/Sun Koshi River Basin in the Central Himalayas. Mt. Res. Dev. 35 (4), 351.

Kim, J.H., 2009. Estimating classification error rate: repeated cross-validation, repeated hold-out and bootstrap. Comput. Stat. Data Anal. 53 (11), 3735–3745.

King, O., Bhattacharya, A., Bhambri, R., et al., 2019. Glacial lakes exacerbate Himalayan glacier mass loss. Sci. Rep. 9 (1), 18145.

Kumar, A., Mal, S., Schickhoff, U., et al., 2025. Basin-scale spatio-temporal development of glacial lakes in the Hindukush-Karakoram-Himalayas. Global Planet. Change 245, 104656.

Lehner, B., Beames, P., Mulligan, M., et al., 2024. The Global Dam Watch database of river barrier and reservoir information for large-scale applications. Sci. Data 11 (1), 1069.

Lesi, M., Nie, Y., Shugar, D.H., et al., 2022. Landsat- and Sentinel-derived glacial lake dataset in the China–Pakistan Economic Corridor from 1990 to 2020. Earth Syst. Sci. Data 14 (12), 5489–5512.

Lesi, M., Nie, Y., Wang, W., et al., 2026. Monitoring Glacier debris flows and dammed Lakes using multiple satellite images in the badswat watershed, Northern Karakoram. Remote Sens. 18 (1), 75.

Liu, M., Chen, N., Zhang, Y., et al., 2020. Glacial lake inventory and lake outburst flood/debris flow hazard assessment after the Gorkha earthquake in the Bhote Koshi Basin. Water 12 (2), 464.
Liu, H., Wang, Z., Wen, H., et al., 2025. Predicting glacial lake outburst susceptibility on the southern Tibetan Plateau with historical events and machine learning methods. Nat. Hazards 121 (15), 17677−17705.
Lützow, N., Veh, G., Korup, O., 2023. A global database of historic glacier lake outburst floods. Earth Syst. Sci. Data 15 (7), 2983−3000.
Marzeion, B., Cogley, J.G., Richter, K., et al., 2014. Attribution of global glacier mass loss to anthropogenic and natural causes. Science 345 (6199), 919−921.
Nie, Y., Deng, Q., Pritchard, H.D., et al., 2023. Glacial lake outburst floods threaten Asia's infrastructure. Sci. Bull. 68 (13), 1361−1365.
Nie, Y., Liu, Q., Liu, S., 2013. Glacial lake expansion in the Central Himalayas by Landsat images, 1990−2010. PLoS One 8 (12), e83973.
Nie, Y., Liu, Q., Wang, J., et al., 2018. An inventory of historical glacial lake outburst floods in the Himalayas based on remote sensing observations and geomorphological analysis. Geomorphology 308, 91−106.
Nie, Y., Pritchard, H.D., Liu, Q., et al., 2021. Glacial change and hydrological implications in the Himalaya and Karakoram. Nat. Rev. Earth Environ. 2 (2), 91−106.
Nie, Y., Sheng, Y., Liu, Q., et al., 2017. A regional-scale assessment of Himalayan glacial lake changes using satellite observations from 1990 to 2015. Remote Sens. Environ. 189, 1−13.
Nie, Y., Wang, W., Pritchard, H.D., et al., 2025. Daily imaging from China's HJ-2A/B satellites enables yearly mapping of regional glacial lakes. Adv. Clim. Change Res. 17 (2), 338−346.
Nie, Y., Zhang, Y., Liu, L., et al., 2010. Glacial change in the vicinity of mt. Qomolangma (Everest), central high Himalayas since 1976. J. Geogr. Sci. 20 (5), 667−686.
Qi, M., Liu, S., Wu, K., et al., 2022. Improving the accuracy of glacial lake volume estimation: a case study in the Poiqu basin, Central Himalayas. J. Hydrol. 610, 127973.
Qi, M., Liu, S., Zhao, Z., et al., 2025. A mathematical model to improve water storage of glacial lake prediction towards addressing glacial lake outburst floods. Hydrol. Earth Syst. Sci. 29 (4), 969−982.
Rafiq, M., Romshoo, S.A., Mishra, A.K., et al., 2019. Modelling Chorabari Lake outburst flood, Kedarnath, India. J. Mt. Sci. 16 (1), 64−76.
RGI 7.0 Consortium, 2023. Randolph Glacier Inventory: A Dataset of Global Glacier Outlines. Version 7.0. National Snow and Ice Data Center, Boulder, Colorado USA.
Richardson, S.D., Reynolds, J.M., 2000. An overview of glacial hazards in the Himalayas. Quat. Int. 65−66, 31−47.
Roberts, D.R., Bahn, V., Ciuti, S., et al., 2017. Cross-validation strategies for data with temporal, spatial, hierarchical, or phylogenetic structure. Ecography 40 (8), 913−929.
Rounce, D., Watson, C., McKinney, D., 2017. Identification of hazard and risk for glacial lakes in the Nepal Himalaya using satellite imagery from 2000-2015. Remote Sens. 9 (7), 654.
Roy, A., Qureshi, S., Pande, K., et al., 2019. Performance comparison of machine learning platforms. Informs J Comput 31 (2), 207−225.
Sattar, A., Cook, K.L., Rai, S.K., et al., 2025. The Sikkim flood of October 2023: drivers, causes, and impacts of a multihazard cascade. Science 387 (6740), eads2659.
Saunier, S., Northrop, A., Lavender, S., et al., 2017. Bulk processing of the Landsat MSS/TM/ETM plus archive of the European Space Agency: an insight into the Level 1 MSS processing. In: 9th International Workshop on the Analysis of Multitemporal Remote Sensing Images (MultiTemp). IEEE.
Shah, J., Hu, J., Edelenbosch, O.Y., et al., 2025. Global dataset combining open-source hydropower plant and reservoir data. Sci. Data 12 (1), 646.
Shen, J., Tan, F., 2020. Effects of DEM resolution and resampling technique on building treatment for urban inundation modeling: a case study for the 2016 flooding of the HUST campus in Wuhan. Nat. Hazards 104 (1), 927−957.
Shrestha, F., Steiner, J.F., Shrestha, R., et al., 2023. A comprehensive and version-controlled database of glacial lake outburst floods in High Mountain Asia. Earth Syst. Sci. Data 15 (9), 3941−3961.
Shugar, D.H., Burr, A., Haritashya, U.K., et al., 2020. Rapid worldwide growth of glacial lakes since 1990. Nat. Clim. Change 10 (10), 939−945.
Song, C., Fan, C., Ma, J., et al., 2025. A spatially constrained remote sensing-based inventory of glacial lakes worldwide. Sci. Data 12 (1), 464.
Subba, S., Ma, Y., Ma, W., et al., 2024. Extreme precipitation detection ability of four high-resolution precipitation product datasets in hilly area: a case study in Nepal. Adv. Clim. Change Res. 15 (3), 390−405.
Taylor, C., Robinson, T.R., Dunning, S., et al., 2023. Glacial lake outburst floods threaten millions globally. Nat. Commun. 14 (1), 487.
Trisakti, B., Julzarika, A., 2011. DEM generation from stereo ALOS PRISM and its quality improvement. Int. J. Remote Sens. Earth Sci. 8 (1), 41−48.
Wang, S., Che, Y., Xinggang, M., 2020a. Integrated risk assessment of glacier lake outburst flood (GLOF) disaster over the Qinghai-Tibetan Plateau (QTP). Landslides 17 (12), 2849−2863.
Wang, X., Guo, X., Yang, C., et al., 2020b. Glacial lake inventory of High-Mountain Asia in 1990 and 2018 derived from Landsat images. Earth Syst. Sci. Data 12 (3), 2169−2182.
Wang, J., Sheng, Y., Tong, T.S.D., 2014. Monitoring decadal lake dynamics across the Yangtze Basin downstream of Three Gorges Dam. Remote Sens. Environ. 152, 251−269.
Wangchuk, S., Bolch, T., 2020. Mapping of glacial lakes using Sentinel-1 and Sentinel-2 data and a random forest classifier: strengths and challenges. Sci. Remote Sens. 2, 100008.
Wangchuk, S., Bolch, T., Robson, B.A., 2022. Monitoring glacial lake outburst flood susceptibility using Sentinel-1 SAR data, Google Earth Engine, and persistent scatterer interferometry. Remote Sens. Environ. 271, 112910.
Watson, C.S., Carrivick, J., Quincey, D., 2015. An improved method to represent DEM uncertainty in glacial lake outburst flood propagation using stochastic simulations. J. Hydrol. 529, 1373−1389.
Wenger, S.J., Olden, J.D., 2012. Assessing transferability of ecological models: an underappreciated aspect of statistical validation. Methods Ecol. Evol. 3 (2), 260−267.
White, N.M., Balasubramaniam, T., Nayak, R., et al., 2022. An observational analysis of the trope "A *p*-value of <0.05 was considered statistically significant" and other cut-and-paste statistical methods. PLoS One 17 (3), e0264360.
Wu, S., Yan, J., Zhang, Y., et al., 2022. Evolutionary process and development implications of traditional trade routes in the Himalayan region. J. Geogr. Sci. 32 (9), 1847−1865.
Wu, Y., Nie, Y., Ahmed, F., et al., 2025. A new approach automatically calculating the outlet and upper catchment area of alpine glacial lakes. J. Hydrol. 651, 132591.
Xu, W., Li, J., Peng, D., et al., 2024. Vertical accuracy assessment and improvement of five high-resolution open-source digital elevation models using ICESat-2 data and random forest: case study on Chongqing, China. Remote Sens. 16 (11), 1903.
Yang, K., Jiang, Y., Tang, W., et al., 2025. A high-resolution near-surface Meteorological Forcing Dataset for the Third Pole Region (TPMFD, 1979−2023). Third Pole Environment Data Center.
Yang, L., Lu, Z., Ouyang, C., et al., 2023. Glacial lake outburst flood monitoring and modeling through integrating multiple remote sensing methods and HEC-RAS. Remote Sens. 15 (22), 5327.
Yao, T., Thompson, L., Yang, W., et al., 2012. Different glacier status with atmospheric circulations in Tibetan Plateau and surroundings. Nat. Clim. Change 2 (9), 663−667.
Yao, T., Xue, Y., Chen, D., et al., 2019. Recent third pole's rapid warming accompanies cryospheric melt and water cycle intensification and interactions between monsoon and environment: multidisciplinary approach with observations, modeling, and analysis. Bull. Am. Meteorol. Soc. 100 (3), 423−444.

Yildiz, O.T., 2013. Omnivariate rule induction using a novel pairwise statistical test. IEEE Trans. Knowl. Data Eng. 25 (9), 2105−2118.

Zhang, G., Yao, T., Chen, W., et al., 2019. Regional differences of lake evolution across China during 1960s−2015 and its natural and anthropogenic causes. Remote Sens. Environ. 221, 386−404.

Zhang, G., Bolch, T., Yao, T., et al., 2023a. Underestimated mass loss from lake-terminating glaciers in the greater Himalaya. Nat. Geosci. 16 (4), 333−338.

Zhang, H., Nie, Y., Liu, L., et al., 2026. An advanced deep learning framework for mapping glacial lakes and its application in the Hindu Kush-Karakoram-Himalaya region. J. Hydrol. 664, 134507.

Zhang, S., Nie, Y., Zhang, H., 2024. Glacial lake changes and risk assessment in Rongxer Watershed of China−Nepal Economic Corridor. Remote Sens. 16 (4), 725.

Zhang, T., Wang, W., An, B., et al., 2023b. Enhanced glacial lake activity threatens numerous communities and infrastructure in the Third Pole. Nat. Commun. 14 (1), 8250.

Zheng, G., Allen, S.K., Bao, A., et al., 2021. Increasing risk of glacial lake outburst floods from future Third Pole deglaciation. Nat. Clim. Change 11 (5), 411−417.

Zhou, B., Zou, Q., Jiang, H., et al., 2024. Process-driven susceptibility assessment of glacial lake outburst debris flow in the Himalayas under climate change. Adv. Clim. Change Res. 15 (3), 500−514.